

Particle acceleration at oblique shocks and discontinuities of the density profile

U.D.J. Gieseler^{1,*}, J.G. Kirk¹, Y.A. Gallant², and A. Achterberg²

¹ Max-Planck-Institut für Kernphysik, Postfach 10 39 80, D-69029 Heidelberg, Germany

² Sterrenkundig Instituut Utrecht, Postbus 80 000, 3508 TA Utrecht, The Netherlands

Received 28 October 1998 / Accepted 8 February 1999

Abstract. In the theory of diffusive acceleration at oblique shock fronts the question of the existence of a discontinuity of energetic particle density is contentious. The resolution of this problem is interesting from a theoretical point of view, and potentially for the interpretation of observations of particle densities at heliospheric shocks and of high-resolution radio observations of the rims of supernova remnants. It can be shown analytically that an isotropic particle distribution at a shock front implies continuity of the particle density – whether or not the shock is oblique. However, if the obliquity of the shock induces an anisotropy, a jump is permitted. Both semi-analytic computations and Monte-Carlo simulations are used to show that, for interesting parameter ranges, a jump is indeed produced, with accelerated particles concentrated in a precursor ahead of the shock front.

Key words: acceleration of particles – shock waves – methods: numerical – ISM: cosmic rays – ISM: supernova remnants

1. Controversy – general description

In the test-particle theory of diffusive shock acceleration, the phase-space spectral index s of accelerated particles depends solely on the compression ratio $r = \rho'/\rho$ of the shock (where ρ and ρ' are the upstream and downstream densities respectively): $s = 3r/(r - 1)$, which results in $s = 4$ for a strong shock in an ideal gas with $c_p/c_v = 5/3$ (Axford et al. 1977; Krymskii 1977; Bell 1978; Blandford & Ostriker 1978). This result, like many other analytical predictions (for a review see Drury 1983; Blandford & Eichler 1987), depends on the assumption that the phase space density is close to being isotropic, even at the shock front. In this case, the density profile of accelerated test particles is a continuous function of position (e.g., Kirk et al. 1994, page 262). In planar symmetry, the density is constant downstream and drops off exponentially upstream of the shock. This situation applies to both parallel and oblique shocks, as was pointed out by, for example, Axford (1981).

Recently, a discussion has arisen in the literature concerning the occurrence of discontinuities in the density of accelerated particles at an oblique shock front. Whereas Ostrowski (1991) (hereafter O91) finds a substantial effect, Naito & Takahara (1995) (hereafter N&T95) assert that the density is continuous. Both of these papers present Monte-Carlo simulations of particle acceleration in which the velocity of the shock front is a significant fraction of the speed of light, and take explicit account of a possible anisotropy of the particle distribution. From the theory of diffusion, it is well-known that the anisotropy of particles of speed v is of the order of u/v , where u is the speed at which the shock sweeps through the medium responsible for making the particles diffuse. At an oblique shock front, the speed relevant for particles diffusing along a magnetic field line is the velocity of the intersection point of the shock front and a given field line, $u = u_s/\cos\Phi$, where u_s is the inflow speed along the shock normal and Φ is the angle between the shock normal and the magnetic field, measured in the upstream rest frame of the plasma. Thus, if the field is oblique, even a relatively slow shock front can produce a substantial anisotropy. The question which we address in this paper is whether or not this anisotropy leads to a discontinuity in the particle density and under what conditions such an effect could be observed.

An approximation which is often used in treating oblique shocks is that in which a particle crossing the shock conserves its magnetic moment (also referred to as the first adiabatic invariant; e.g., Webb et al. 1983). This approximation is valid for non-relativistic perpendicular shocks (Whipple et al. 1986). Terasawa (1979) and Decker (1988) have performed numerical simulations which confirm its accuracy at non-relativistic oblique shocks and Begelman & Kirk (1990) have conducted tests at relativistic shocks. It is important to bear in mind, however, that this approximation breaks down for sufficiently fast shocks (see, for example, Kirk et al. 1994, page 241). Conservation of magnetic moment implies that a particle can be reflected by the magnetic compression at a fast-mode shock front, and the question of the existence of a discontinuity in the particle density is intimately connected with the phenomenon of reflection, as pointed out in an early paper on this subject (Achterberg & Norman 1980). If this approximation is adopted, the problem of acceleration at an oblique shock of particles which undergo pitch-angle diffusion along field lines can be solved semi-analytically

Send offprint requests to: gieseler@msi.umn.edu

* Present address: University of Minnesota, Department of Astronomy, 116 Church St. S.E., Minneapolis, MN 55455, USA

(Kirk & Heavens 1989, hereafter K&H89), at least for the case in which the accelerated particles are ultra-relativistic ($v = c$) and build a power-law distribution in momentum. In Sect. 3, we address the question of the existence of a discontinuity using a new Monte-Carlo code incorporating the assumption of conservation of magnetic moment (Gieseler 1998). Since there already exist contradictory simulations in the literature, we take particular care to check the results obtained with this new code against the analytic results of K&H89. Both the code and the analysis find a discontinuity. However, although N&T95 also adopted the assumption of conservation of magnetic moment in their simulations, they did not find a discontinuity. We show that this can be caused by low spatial resolution of the simulation and does not necessarily invalidate results concerning the spectrum of accelerated particles. Ostrowski (1991), on the other hand, *did* find a discontinuity, without implementing the conservation of magnetic moment. In Sect. 2 we argue that Liouville's theorem in fact guarantees continuity in this case. This result can once again be caused by a rapidly varying density profile which is sampled at low spatial resolution; in this case it appears because the length scale of a gyration radius was not resolved. However, Ostrowski's results do indicate that the accumulation of particles upstream of a relativistic shock front is an important physical effect, even though there may not be a discontinuity in the strict sense.

At non-relativistic shocks, such as those observed in the solar system, the analytic method of K&H89 fails, and one must rely on simulations. Here again the situation is not clear-cut. Monte-Carlo simulations by Ellison et al. (1996) do not show discontinuities or a jump across the shock front, whereas recent numerical solutions using the finite difference method have found such effects (Ruffolo 1999). In Sect. 3.3 we present high resolution test-particle simulations using parameters appropriate for solar system shocks and demonstrate the existence of accumulated particles in the precursor of the shock.

The resolution of this question is not only of formal interest, but is also relevant for the interpretation of data taken by the Ulysses spacecraft and of observations of the radio emission of supernova remnants. These applications are discussed briefly in Sect. 4.

2. Analytical considerations

The system we consider consists of energetic particles which move in two half-spaces separated by a shock front. Plasma flows into and out of the shock front carrying with it a uniform magnetic field. In addition to the uniform field, we assume there exist magnetic fluctuations static in the rest frame of the plasma on each side of the shock whose effect on the particle motion may be described via a scattering operator. Two levels of approximation are important. In the first, the particle is described by its full six-dimensional phase space coordinates. The trajectory is integrated in an explicit realisation of the stochastic magnetic field, taking full account of the gyration phase. Upon crossing the shock front, the trajectory experiences no forces other than those exerted by the magnetic field. This is the approach used by

O91. The second level of approximation is one in which the particle is described by five coordinates: the position of the guiding centre, the magnitude of the momentum and the pitch angle. The magnetic field is assumed uniform and the guiding centre follows a field line except when crossing the shock. The magnetic moment is conserved in between scattering events, which are assumed to change only the pitch angle, and also upon crossing the shock front. This is the approximation used by K&H89 and N&T95. It is generally referred to in the literature as the 'drift approximation', and we adopt this terminology here, although we do not explicitly consider the drifts themselves.

In both levels of approximation a discontinuity can in principle arise in the formal description of the dependence of the distribution function on the spatial coordinate along the shock normal. However, the physical interpretation of a mathematical discontinuity is different in each case.

In the first approximation, the shock front is taken to have zero thickness. In reality, the shock transition will extend over a finite region in space, which is assumed to be small compared to the other length scales of interest, for example the gyration radius of the energetic particles. Thus, if the acceleration process were to produce a significant change in the energetic particle density over a length scale smaller than the gyration radius, but perhaps comparable to the shock thickness, this would appear as a discontinuity in simulations such as those of O91. However, since particles do not suffer impulsive deflection at the shock front, i.e., the momentum coordinates of a particle are in general continuous functions of position even at the shock front itself, it follows from Liouville's theorem that the phase-space distribution function, which is constant along trajectories, is also a continuous function of position across the shock front. The particle density is simply an integral of this function over all momenta, so that it is also continuous, provided the momentum is measured in the same frame of reference both upstream and downstream of the shock. Thus, there can be no formal discontinuity in this approach. Of course, the density may vary smoothly on the length scale of the gyration radius, so that we can interpret Ostrowski's result as due to a strong gradient in the density on this length scale.

The drift approximation, however, can only resolve changes which occur on length scales longer than a gyration radius, so that the distribution found by Ostrowski *must* appear as a discontinuity in simulations which use this approximation. There is a close relationship between such a discontinuity and the angular distribution, which can be understood as follows. Consider an oblique shock viewed in the de Hoffmann-Teller (hereafter dHT) frame (de Hoffmann & Teller 1950; Kirk et al. 1994), in which the electric field vanishes and the shock is stationary. A particle trajectory is now described by only five coordinates, of which the magnetic moment is conserved both between scatterings and on encountering the shock front. Denoting by p_{\perp} the component of the particle momentum perpendicular to the magnetic field \mathbf{B} , the magnetic moment is p_{\perp}^2/B . Because $p = |\mathbf{p}|$ is also conserved in the dHT frame (in which the electric field vanishes) this leads to

$$\frac{1 - \mu^2}{B} = \frac{1 - (\mu')^2}{B'}, \quad (1)$$

where a prime denotes downstream quantities. Rearranging, the downstream pitch angle is given by

$$\mu' = (\mu/|\mu|) \sqrt{(\mu^2 - \mu_{\text{crit}}^2)/(1 - \mu_{\text{crit}}^2)}, \quad (2)$$

where the cosine of the of the loss-cone angle is given by $\mu_{\text{crit}} = \sqrt{1 - B/B'}$. Thus, according to its pitch angle, an upstream particle may be reflected or transmitted, and we can divide phase space on the upstream side of the shock into four regions:

- (a) $\mu_{\text{crit}} < \mu < 1$, particles approaching the shock which will be transmitted (i.e., in the loss cone);
- (b) $0 < \mu < \mu_{\text{crit}}$, particles approaching the shock which will be reflected;
- (c) $-\mu_{\text{crit}} < \mu < 0$, particles leaving the shock after reflection;
- (d) $-1 < \mu < -\mu_{\text{crit}}$, particles leaving the shock after transmission from downstream.

The phase space downstream splits into just two regions, $\mu' > 0$ and $\mu' < 0$, since no trajectories incident from downstream are reflected.

In the drift approximation, the phase-space distribution function is independent of gyration phase to lowest order (e.g., Spatschek 1990, page 145), so that application of Liouville's theorem yields

$$f(p, \mu) = f(p, -\mu) \quad \text{for } |\mu| < \mu_{\text{crit}} \quad (\text{reflection}), \quad (3)$$

$$f(p, \mu) = f'(p, \mu') \quad \text{for } |\mu| > \mu_{\text{crit}} \quad (\text{transmission}), \quad (4)$$

where conservation of the momentum p in the dHT frame is used.

The upstream and downstream densities are given by

$$n = \int_{-1}^{-\mu_{\text{crit}}} d\mu n_t(\mu) + \int_{-\mu_{\text{crit}}}^{\mu_{\text{crit}}} d\mu n_r(\mu) + \int_{\mu_{\text{crit}}}^1 d\mu n_t(\mu), \quad (5)$$

$$n' = \int_{-1}^1 d\mu' n'_t(\mu'), \quad (6)$$

where we have defined the quantities

$$n_{t,r}(\mu) := \int f(p, \mu) 2\pi p^2 dp, \quad (7)$$

$$n'_t(\mu') := \int f'(p, \mu') 2\pi p^2 dp = n_t(\mu), \quad (8)$$

such that the suffix r refers to particles which are or will be reflected (i.e., $|\mu| < \mu_{\text{crit}}$) and the suffix t to ones which are or will be transmitted ($|\mu| > \mu_{\text{crit}}$, or $-1 < \mu' < 1$). The second relation in Eq. (8) follows from Eq. (4).

A continuous density distribution at the shock front ($n = n'$) is in general not guaranteed. This can be seen by using specific assumptions about the density of transmitted and reflected particles and Eqs. (5)–(6) (Gieseler 1998). For the physical distribution of Fig. 4, the values of the density which can be calculated

from Eq. (5) and Eq. (6) are quite different, as discussed below. The reason for the upstream and downstream densities to be different can be understood from Eq. (8), which preserves a ‘balance’ of the transmitted particles, whereas the reflected particles contribute only to the upstream density. A continuous density is obtained if there is no compression of the magnetic field ($B = B'$). In this case no particles are reflected ($\mu_{\text{crit}} = 0$) and Eqs. (5)–(8) then give $n = n'$. This is valid for a parallel shock and the trivial case in which no shock front is present. If the pitch-angle distribution is isotropic at an oblique shock front, then one again finds $n = n'$ by integration of Eqs. (5) and (6). Noting that in this case $n_t(\mu)$ and $n_r(\mu)$ have the same constant value, continuity follows from Eq. (8). In other words, the contribution of the reflected particles upstream exactly balances the compression of the transmitted ones downstream in this case.

To summarise this section, in general the density of accelerated test particles at oblique shocks will vary on the length scale of the gyration radius across the shock front. This variation is closely connected with the anisotropy of the angular distribution. It should appear as a discontinuity in treatments which use the drift approximation to the particle motion. However, when conditions are such that the theory of diffusive acceleration applies, i.e., the particle velocity is much larger than the shock speed projected along the magnetic field ($v \gg u_s / \cos \Phi$), then the anisotropy and the associated density variation are small.

3. Monte-Carlo simulations

We now present results from test-particle simulations of accelerated particles at shock fronts. The key aspects of the technique have been used and described by several authors (e.g., Kirk & Schneider 1987; O91; Baring et al. 1993; N&T95), so that a brief description suffices. We consider oblique shocks, where the magnetic field is inclined at an angle Φ with respect to the shock normal in the upstream rest frame, and has no dynamical effect on the plasma flow. The shock speed in this frame is u_s . We consider (in principle) the whole range of Φ for subluminal shocks, e.g. $u_s \leq u_s / \cos \Phi < 1$ (here and below: $c = 1$). The gyration centre of a particle's trajectory is followed in the upstream and downstream rest frames of the background plasma. In these frames, as in the dHT frame, the momentum $p = |p|$ is constant. Particles move along the magnetic field under the influence of small scale irregularities which lead to pitch-angle scattering. We do not investigate the effect of transport of particles perpendicular to the mean magnetic field. We use an algorithm for calculating a pitch angle μ_{new} from a given pitch angle μ which was given by O91 (see Fig. 1 therein). From two random numbers R_1 and R_2 which are uniformly distributed on the interval $[0, 1]$, the new pitch angle is given by

$$\cos \Delta\Omega = 1 - (1 - \cos \Delta\Omega_{\text{max}}) R_1, \quad (9)$$

$$\mu_{\text{new}} = \mu \cos \Delta\Omega + \sqrt{1 - \mu^2} \sin \Delta\Omega \cos(2\pi R_2), \quad (10)$$

where we have chosen $\Delta\Omega_{\text{max}} = 0.1$ for most of the simulations shown below. This gives a very good approximation of pitch-angle scattering with an infinitesimal amplitude. The results (at

least for the spectral index and the density distribution) do not change substantially for a factor of 5 higher or lower value of $\Delta\Omega_{\max}$.¹ The time step Δt for successive scatterings is kept constant. These scatterings are performed in the upstream and downstream rest frames. At a shock crossing, we transform the particle momentum p and the pitch angle μ into the dHT frame, which is always possible at subluminal oblique shocks (for a description of the Lorentz transformations between these frames see K&H89 or Gieseler 1998), and apply the conservation of magnetic moment (Eq. 1) to find the new downstream pitch angle in the dHT frame. Transformation into the downstream rest frame then gives the new values of the momentum and pitch angle. This method is also used by K&H89 and N&T95, to which we compare our results.

The validity of the assumption of conservation of the magnetic moment can be evaluated as follows. First, consider a ‘strict’ condition which can be applied to a single particle crossing the shock (Kirk et al. 1994, page 241). The number of times a trajectory intersects the shock front can be estimated as

$$N_{\text{cross}} \approx \tan \alpha \tan \Phi_{\text{dHT}}, \quad (11)$$

where $\alpha = \cos^{-1} \mu$ is the pitch angle, and Φ_{dHT} is the angle between the upstream field and the shock normal measured in the dHT frame.² Adiabatic behaviour is expected when $N_{\text{cross}} \gg 1$. An accurate separation between transmitted and reflected particles is guaranteed if we demand this condition to be valid for at least all particles outside the loss cone, i.e., $|\mu| \leq \mu_{\text{crit}} \equiv \cos \alpha_{\text{crit}} = \sqrt{1 - B/B'}$, where $B/B' = [(1 + \tan^2 \Phi_{\text{dHT}})/(1 + r^2 \tan^2 \Phi_{\text{dHT}})]^{-1/2}$ and r is the compression ratio. Inserting the critical pitch angle α_{crit} in Eq. (11) and expanding in powers of $1/N_{\text{cross}}$, we get a condition for the upstream inclination angle in the dHT frame which is independent of the fluid speed:

$$\tan \Phi_{\text{dHT}} \gg \sqrt{r - 1}. \quad (12)$$

For the non-relativistic shock speed $u_s = 0.01$, Eq. (12) is fulfilled for essentially the whole parameter range in $u_s/\cos \Phi$ considered here. For shock speeds in the mildly relativistic region, Eq. (12) always holds in an (albeit small) region at $u_s/\cos \Phi \rightarrow 1$.

The condition $N_{\text{cross}} \gg 1$ is, however, much too strict. A less conservative approach is to assume validity of the approximation in an average (over phases) sense. This has been shown by simulations as mentioned above. For example Decker (1988) finds that for non-relativistic shocks the results compare well with adiabatic behaviour over the whole range of Φ . In particular, the data shown in his Fig. 8 show close agreement concerning the reflection probability for the approximate and numerical results. Ostrowski (1991) used an extended Monte-Carlo code which does not assume adiabatic behaviour. He was thus able to check the quality of the approximation at mildly relativistic shock speeds. His Fig. 3 shows good agreement with K&H89

for the spectral index. Departures start to occur at $u_s = 0.5$, but always diminish as $u_s/\cos \Phi \rightarrow 1$. Furthermore, we have directly compared our simulations with his for $u_s = 0.3$ at $\Phi = 60^\circ$ and 70° and found the same density discontinuity (see below).

To test the accuracy of our scheme against the calculation of K&H89, particles are injected in the upstream plasma with a velocity corresponding to $\gamma v = p/m \geq 2$, which means that they are already relativistic at injection. For intersection speeds of shock and magnetic field of $u_s/\cos(\Phi) \geq 0.9$ the injection momentum has to be even higher. We are interested in particles with momenta where the distribution has attained a pure power law, and especially in the spectral index of this power law. Only particles from the power-law region in the momentum distribution are used for the pitch-angle and density distributions. Within this region we found that the angular distribution is independent of the momentum range chosen, and the power-law index is thus independent of angle. Simulation of an individual particle terminates when a maximum momentum is reached (two orders of magnitude higher than the upper limit of Fig. 1), or when the particle reaches a distance from the shock on the downstream side which is three times greater than the left boundary of Fig. 5, at which the density distribution has already reached its constant downstream value. These limits vary with the parameters u_s and Φ , and were always chosen such that boundary effects are not important. The results from Monte-Carlo simulations and semi-analytical computations are shown (with the exception of Fig. 8) for a compression ratio of $r = 4$.

The three main aspects of the results are spectral index, angular distribution and spatial distribution, and these are presented in turn.

3.1. Spectral index

The momentum distribution of particles is measured at the shock front in the upstream rest frame. An example is shown in Fig. 1, where 10^6 independent particles were simulated. The plot also contains a fit to the function $y = 10^{p_1 + p_2 x}$, together with the values of the fit parameters and their statistical errors. The spectral index can be calculated from $\Delta N/\Delta \log(p/m) \propto p^{-s+3}$; this gives $s = 3 - p_2$. The statistical error of the fit to the spectra is less than 1% for all spectral indices discussed below. To achieve maximum accuracy from the Monte-Carlo simulations, we fit the spectrum over a large finite range of momentum and did not include loss mechanisms. For $s < 3.2$ the statistical errors are less than 0.1%. For spectral indices near $s \simeq 3$ the statistics are very much better, because particles then gain energy mainly due to reflection. This means that not much time is taken in following the particle trajectories in those parts of the downstream region where the particle has a low chance of returning to the shock front. As a result, the error in s is less than 0.01% for spectral indices corresponding to $u_s/\cos \Phi > 0.8$. Fig. 2 shows the spectral indices for non-relativistic and mildly relativistic shock velocities and a wide range of inclination an-

¹ O91 used $\Delta\Omega_{\max} = 0.3$ as an approximation for infinitesimal pitch-angle scattering.

² Note that $\cos^2 \Phi = (1 + u_s^2 \tan^2 \Phi_{\text{dHT}})/(1 + \tan^2 \Phi_{\text{dHT}})$.

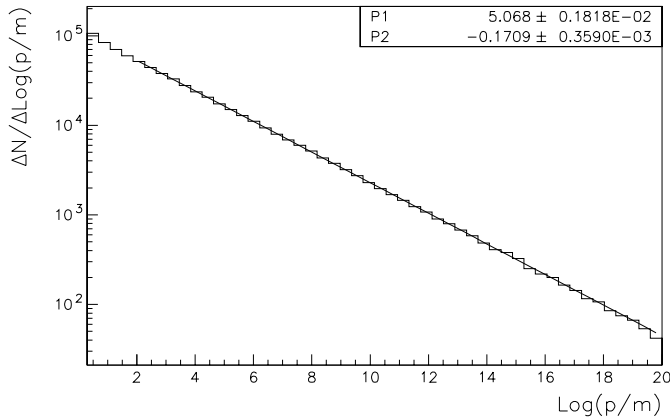


Fig. 1. Monte-Carlo simulation of a momentum spectrum for compression ratio $r = 4$, shock speed $u_s = 0.4$ and an angle of the magnetic field of $\Phi = 45^\circ$. The speed of the intersection of magnetic field and shock is then $u_s / \cos \Phi = 0.5657$ (same parameters as for Fig. 4 and Fig. 5). The spectral index of the phase space density is $s = 3.1709 \pm 0.0004$.

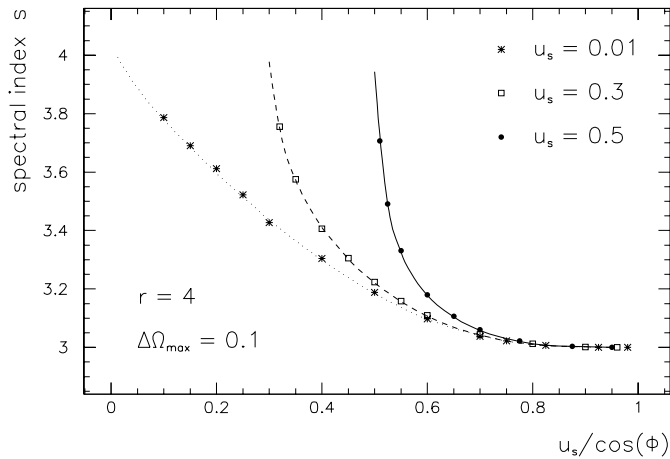


Fig. 2. Comparison of the spectral index from Monte-Carlo simulations for infinitesimal pitch-angle scattering with $\Delta\Omega_{\max} = 0.1$ (dots, stars, squares) with semi-analytical results from K&H89 (solid line: $u_s = 0.5$; dashed line: $u_s = 0.3$; dotted line: $u_s = 0.01$).

gles Φ . The lines in this plot are taken from Fig. 2 and Fig. 6 of K&H89 and are in precise agreement with the simulations.

Very important for an understanding of the spectral index and the density profile is the effect of the underlying scattering law. The results become quite different for isotropisation after each scattering, given by $\Delta\Omega_{\max} = \pi$. Although this does not correspond exactly to the simulation of large-angle scattering on point-like scattering centres (for which it would be necessary to choose exponentially distributed time steps, and consider cross field diffusion), the effects it produces should be qualitatively similar. Using a scattering law in the transition regime between infinitesimal pitch-angle scattering and isotropisation after each scattering allows an investigation of this dependence. We focus on one example with $\Delta\Omega_{\max} = 1.0$ (intermediate pitch-angle scattering). This kind of scattering can have a very big influence on the precursor of accelerated par-

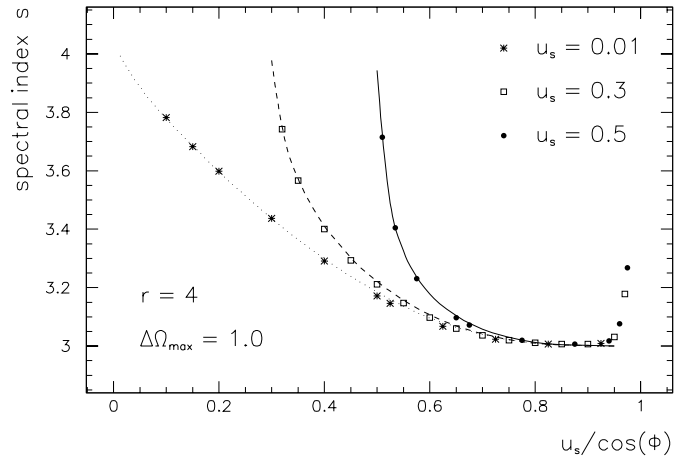


Fig. 3. Comparison of the spectral index for *intermediate* pitch-angle scattering with $\Delta\Omega_{\max} = 1.0$ from Monte-Carlo simulations (dots, stars, squares) with *infinitesimal* pitch-angle scattering (lines) which are semi-analytical results from K&H89 (solid line: $u_s = 0.5$; dashed line: $u_s = 0.3$; dotted line: $u_s = 0.01$).

ticles. Under pitch-angle scattering with $\Delta\Omega_{\max} \gtrsim 1$ particles have a higher escape probability from the shock because they are free to change their pitch angle to a value in the loss cone ($\mu_{\text{crit}} < \mu < 1$) within a few scatterings, and may then be transmitted through the shock. This reduces the upstream density, as we will see later, but also leads to a steeper spectrum for accelerated test particles. Fig. 3 shows a comparison of the spectral index for intermediate and infinitesimal pitch-angle scattering. The stars, squares and dots show Monte-Carlo results for intermediate pitch-angle scattering with $\Delta\Omega_{\max} = 1.0$, whereas the lines are (as in Fig. 2) results from K&H89 for infinitesimal pitch-angle scattering ($\Delta\Omega_{\max} \ll 1$). It can be seen that even for a relatively large value of $\Delta\Omega_{\max} = 1.0$, the effect is very small for most intersection velocities of magnetic field and shock.

For infinitesimal pitch-angle scattering and $u_s / \cos \Phi > 0.8$, a flat $s \simeq 3$ spectrum is achieved. In the standard picture, this spectrum corresponds to acceleration with vanishing escape probability. Here it is associated with a very strong pile-up (see Fig. 6). A large (~ 1) value of $\Delta\Omega_{\max}$ reduces the pile-up (see Fig. 7) and effectively increases the escape probability, leading to the steeper spectrum shown in Fig. 3 for $u_s / \cos \Phi > 0.95$. For $\Delta\Omega_{\max} = \pi$ (isotropisation at each scattering) the spectrum becomes steeper for all inclination angles. This point was noted by N&T95 (their Fig. 7), and our results for the spectral index are in good agreement with theirs.

3.2. Pitch-angle distribution

As shown in Sect. 2, the pitch-angle distribution of accelerated particles plays a crucial role in determining whether the density distribution has a jump at the shock front. For every set of parameters we have measured the pitch-angle distribution and present an example of the results in Fig. 4. The lines represent the distributions calculated semi-analytically by K&H89, whereas the discrete symbols show the contents of the ‘bins’ filled in the

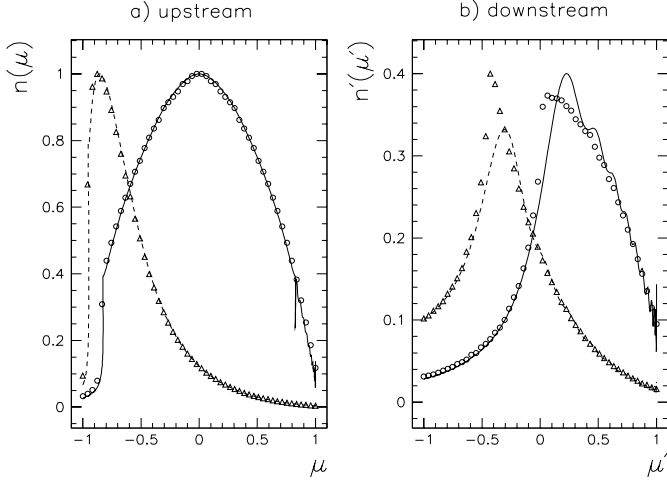


Fig. 4a and b. Pitch-angle distribution at the shock front for $\Delta\Omega_{\max} = 0.1$ and compression ratio $r = 4$. **a** and **b** show the distribution at the upstream and downstream side of the shock. In each figure the lines are from K&H89 and the discrete symbols display the ‘bins’ of the Monte-Carlo simulations. The solid lines and the circles show the distribution in the dHT frame, and the dashed lines and the triangles show the distributions in the upstream **a** and downstream **b** rest frame. See text for the normalisation. The shock speed is $u_s = 0.4$, and the upstream inclination angle of the magnetic field $\Phi = 45^\circ$ (compare Fig. 1 and Fig. 5).

above described Monte-Carlo method. The four representations of the pitch-angle distribution at the shock shown in Fig. 4 are: 1. Upstream of the shock in the upstream rest frame (Fig. 4a dashed line and open triangles). 2. Upstream of the shock in the dHT frame (Fig. 4a solid line and open circles). 3. Downstream of the shock in the downstream rest frame (Fig. 4b dashed line and open triangles). 4. Downstream of the shock in the dHT frame (Fig. 4b solid line and open circles). The upstream distributions (Fig. 4a) are normalised to their maximum value. The normalisation at the downstream side of the shock are as follows: the Monte-Carlo distribution in the dHT frame has the same normalisation as the corresponding upstream one, to allow a direct comparison between the two (see below); however, the Monte-Carlo distribution in the downstream rest frame is normalised to a maximal value of 0.4 to enable it to be displayed in the same figure. In each case, the normalisation of the semi-analytical results of K&H89 are chosen to provide the best fit to the Monte-Carlo distributions. Comparison of the pitch-angle distributions from the two methods in Fig. 4 confirms that they are in close agreement.

Particles with pitch angle $\mu > 0$ in the dHT frame move in the downstream direction. From Eq. (1) we can calculate a critical pitch angle cosine below which these particles will be reflected upstream of the shock. For $r = 4$, $\Phi = 45^\circ$ and $u_s = 0.4$ we get $\mu_{\text{crit}} = 0.826$. Reflected particles contribute symmetrically about $\mu = 0$ and constitute the major part of the distribution (see solid line of Fig. 4a), indicating that repeated reflections are effective in keeping particles upstream. The particles with $\mu < -\mu_{\text{crit}} = -0.826$ in the dHT frame are particles

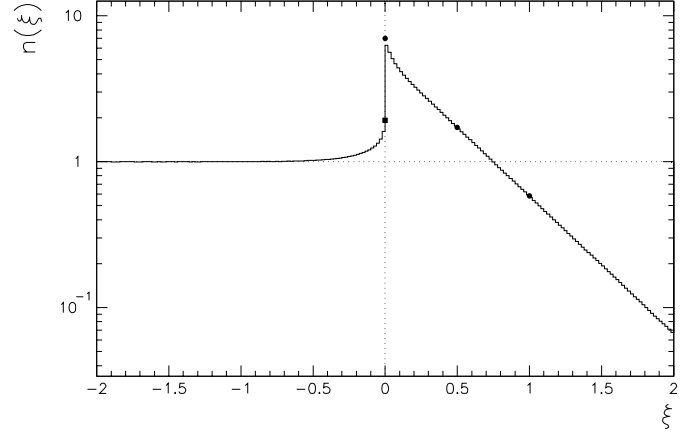


Fig. 5. Monte-Carlo Simulation of the density profile at an oblique shock with compression ratio $r = 4$, maximal scattering angle $\Delta\Omega_{\max} = 0.1$, shock speed $u_s = 0.4$ and inclination angle $\Phi = 45^\circ$ (compare Fig. 1 and Fig. 4). The solid line shows the ‘bins’ of a position measurement of particles, whereas the filled dots show a density measured through the flux through a surface with constant distance upstream of the shock. The filled square indicates a measurement downstream of the shock.

which cross the shock from the downstream side. A Lorentz transformation³ of the critical angle $-\mu_{\text{crit}} = -0.826$ into the upstream rest frame gives $(-\mu_{\text{crit}})^* = -0.949$. At the downstream side of the shock the distribution in the dHT frame (solid line of Fig. 4b) is simply divided into particles going upstream ($-1 \leq \mu < 0$) and those going downstream ($0 < \mu \leq 1$). The boundary $\mu_b = 0$ between these regions is transformed to $\mu_b^* = -0.446$ in the downstream rest frame.

3.3. Density profile

From the pitch-angle distributions one can calculate the density using Eqs. (5) and (6), which is the integration of the pitch-angle distributions in the dHT frame. From Fig. 4 we see that the distribution immediately downstream of the shock is $\lesssim 0.38$ (open circles in Fig. 4b), compared to ≤ 1 for the upstream distribution (open circles in Fig. 4a). By comparing the upstream and downstream distributions in the dHT frame, it is obvious that the downstream integral is less than upstream, and therefore the density is discontinuous at the shock.

In planar symmetry, the density distribution of accelerated test particles is a function of the distance from the shock front. We use the dHT frame in order to compare the densities upstream and downstream directly, as in Sect. 2. In this frame the shock is stationary (at $x = 0$). We normalise the distance x perpendicular to the shock as the dimensionless variable ξ according to

$$\xi = \frac{u_s}{\kappa_{\parallel} \cos^2 \Phi} x, \quad (13)$$

where Φ is the upstream inclination angle of the magnetic field as defined above, and κ_{\parallel} the parallel diffusion coefficient (e.g.

³ For particles with velocity $v = c$.

Jokipii 1971; Skilling 1975; Decker 1988):

$$\kappa_{\parallel} = \frac{v^2}{4} \int_{-1}^1 d\mu \frac{1 - \mu^2}{\nu_s}, \quad \nu_s = \frac{1}{1 - \mu^2} \langle (\Delta\mu)^2 \rangle, \quad (14)$$

where ν_s is the scattering frequency and we have used $v = c$ in the normalisation. Note that κ_{\parallel} , while convenient for the determination of a length scale, does not describe the transport of particles for the anisotropic distributions discussed here. The mean squared variation in μ can easily be calculated from Eqs. (9) and (10). Defining $\delta\mu_0 := \cos(\Delta\Omega_{\max})$, then

$$\langle (\Delta\mu)^2 \rangle = \frac{1}{2}(1 - \delta\mu_0)(1 - \delta\mu_0\mu^2) - \frac{1}{6}(1 - \delta\mu_0)^2. \quad (15)$$

Fig. 5 shows the steady-state density in the dHT frame for a shock with velocity $u_s = 0.4$, compression ratio $r = 4$ and inclination angle $\Phi = 45^\circ$. The upstream plasma velocity in the dHT frame is then $u_s/\cos\Phi = 0.5657$. The plot shows the density $n(\xi)$ as a function of the distance to the shock ξ . Contributions to this density were limited to particles from the power law part of the spectrum, indicated by the fit in Fig. 1. Because the question of spatial resolution is of crucial importance to our discussion, we use two independent methods to evaluate the density. The solid line shows the contents of spatial ‘bins’, where particles simply contribute after every time step to the ‘bin’ at their actual position. These ‘bins’ are located such that the shock lies at the border between two of them. An independent way of measuring the density is to count particles which cross a plane at a certain position. The count rate is proportional to the flux through this plane; to obtain the density, one divides this quantity by the relative velocity of the binned particle and the plane. The shock plane and other planes at constant ξ are stationary in the dHT frame, so that the particle velocity relative to the planes is $v\mu\cos\Phi_{\text{dHT}}$ in the upstream region (see footnote 2 for the relation between Φ and Φ_{dHT}), where the particle velocity v is multiplied by the cosine of the angle with respect to the magnetic field μ and the cosine of the inclination angle of the magnetic field relative to the normal of the plane. The three filled dots at $\xi = 0, 0.5$ and 1 show the density in the upstream region, whereas the filled square shows the density at the downstream side of the shock at $\xi = 0$. In particular, the two values at $\xi = 0$ are calculated from the integration of Eqs. (5) and (6) over the dHT distributions shown in Fig. 4 (open circles). The normalisation is in each case such as to give unity far downstream of the shock.

Both methods display a discontinuous density profile in Fig. 5. However, finite spatial resolution means that the binning method systematically underestimates the value of the density when approaching the shock front from either side. The second method, on the other hand, is a precise measure of the density at $\xi = 0$. For the example of Fig. 5 (10^6 independent particles) we get $n/n' = 3.641 \pm 0.004$, where n represents the filled circle, and n' represents the filled square at $\xi = 0$. Fig. 6 shows the ratio n/n' for various shock velocities and inclination angles. (The number of particles lies between $6 \cdot 10^3$ to $5 \cdot 10^6$ and the statistical error of n/n' is $< 5\%$). For $\Phi = 0$ (parallel shock) we

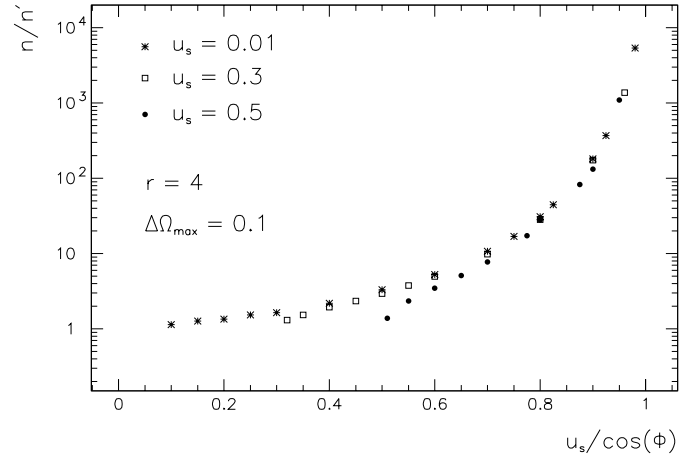


Fig. 6. Ratio of the upstream to the downstream density at the shock front vs. the intersection velocity of the shock and the magnetic field for *infinitesimal* pitch-angle scattering with $\Delta\Omega_{\max} = 0.1$, compression ratio $r = 4$ and three different shock speeds. The values of n/n' are taken from flux measurements at the shock front, exemplified by the filled circle and square at $\xi = 0$ in Fig. 5.

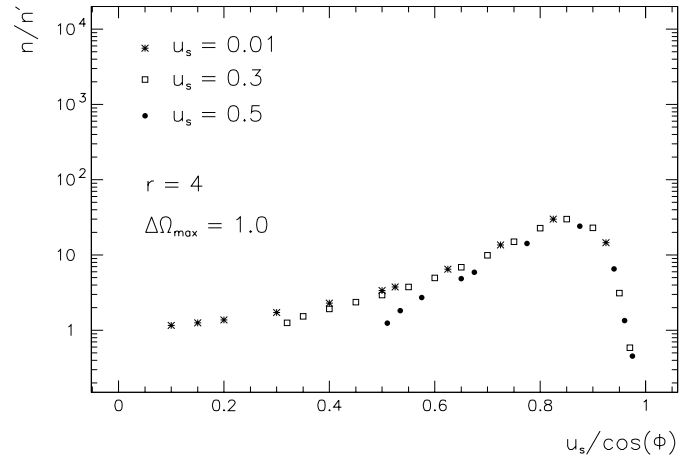


Fig. 7. Ratio of the upstream to the downstream density at the shock front vs. the intersection velocity of the shock and the magnetic field for *intermediate* pitch-angle scattering with $\Delta\Omega_{\max} = 1.0$, compression ratio $r = 4$ and three different shock speeds. The values of n/n' are taken from flux measurements at the shock front. For values of $u_s/\cos\Phi \lesssim 0.8$, the results are essentially the same as those shown in Fig. 6.

get a continuous density ($n = n'$) for all shock speeds, because here no reflection can occur (see Sect. 2). If the velocity of the intersection point of the shock and the magnetic field exceeds 0.8 of the particle velocity (in the case $v = c$ discussed here), the upstream density becomes more than 10 times the downstream density at the shock front. This ratio increases very rapidly for higher intersection velocities. Our calculations are performed for test particles, but in reality such particles may exert a substantial pressure, which would be important in calculations which include the back-reaction of the particles on the flow, as pointed out by O91. However (as discussed in Sect. 3.1), increasing the magnitude of the maximal change in pitch angle ($\Delta\Omega_{\max}$) leads

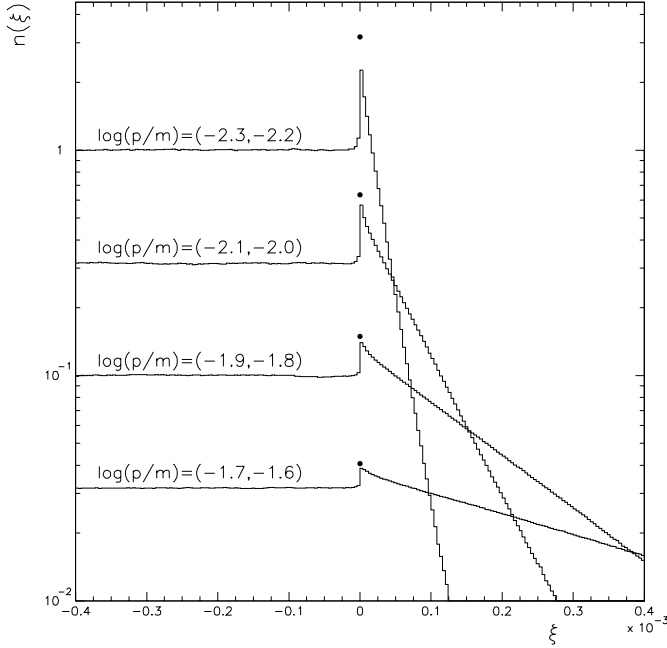


Fig. 8. Monte-Carlo Simulation of the density profile at an oblique shock ($\Phi = 60^\circ$) with compression ratio $r = 3.5$ and shock speed $u_s = 300 \text{ km s}^{-1}$, for various regions of the particle velocity. The normalisation of each plot is chosen to avoid overlap. The maximal scattering angle is $\Delta\Omega_{\text{max}} = 0.5$. The filled dots show the upstream density measured from the flux at the shock and normalised to the value of the corresponding plot far downstream.

to a strong reduction of the highest possible upstream densities. This can be seen very clearly from Fig. 7, where the maximal change in pitch angle is $\Delta\Omega_{\text{max}} = 1.0$, and arises because in this case the angular distribution cannot develop a sharply peaked structure such as that shown in Fig. 4. For isotropisation of the pitch angle after each scattering event, the ratio n/n' for $r = 4$ is always smaller than 2 for all inclination angles which are possible for subluminal oblique shocks ($u_s < \cos \Phi$).

Finally, in Fig. 8 we show the density profile for an oblique shock ($\Phi = 60^\circ$) with non-relativistic shock velocity $u_s = 300 \text{ km s}^{-1}$. We have simulated the acceleration of test particles at an unmodified low Mach-number shock with compression ratio $r = 3.5$, typical for shocks in the solar wind. The pitch-angle scattering is described by Eqs. (9) and (10) with $\Delta\Omega_{\text{max}} = 0.5$. This plot shows the density for 4 different velocity regimes of the accelerated particles, which were injected with velocity $p/m = 2.1 \cdot 10^{-3}$, just higher than the intersection velocity of shock and magnetic field ($u_s/\cos \Phi = 2 \cdot 10^{-3}$). The density is normalised such that overlap of the four plots is avoided. For each plot in Fig. 8 the filled dot represents the density measured at the shock front on the *upstream* side from the flux at the shock plane (compare Fig. 5 and the corresponding text). For the lowest energy particles shown in Fig. 8, which would correspond to protons with a kinetic energy between 12 and 19 keV, the density upstream of the shock exceeds the density far downstream by more than a factor of 3, and the ratio of the density upstream relative to downstream *at* the shock front is given by

$n/n' = 2.81 \pm 0.02$ at this ‘energy band’ (note that the error represents only the statistical fluctuation). It can be seen from Fig. 8 that these ratios depend on the velocity of the particles. If the particle velocity exceeds the velocity of shock and magnetic field intersection by an order of magnitude, the distribution becomes more isotropic and therefore the density jump tends to disappear, as discussed in Sect. 1 and 2.

4. Discussion

We have presented an analysis of particle acceleration at oblique shocks, with special emphasis on the density of accelerated test particles. It was shown analytically that in general a density jump can occur at an oblique shock front. This was done on the basis of Liouville’s theorem and by integrating the phase space density, without the a priori assumption of an isotropic pitch-angle distribution. It turns out that for situations in which the pitch-angle distribution is non-isotropic, a density peak at the shock front can appear. This peak has a discontinuity at the position of the shock, if the adiabatic treatment is used. One can describe the resulting precursor of upstream accelerated particles as due to reflections at the shock front.

We used Monte-Carlo simulations to calculate the spectral index and the pitch-angle distribution. These results are in good agreement with semi-analytical calculations from K&H89. The corresponding density profile shows a pronounced discontinuity for a large range of parameters, which was also found by O91 (see Fig. 6 therein), and our results are quantitatively in very good agreement ($r = 5.28$, $u_s = 0.3$, $\Delta\Omega_{\text{max}} = 0.1$, $u_s/\cos \Phi = 0.6 \Rightarrow n/n' = 6.31 \pm 0.04$; and $u_s/\cos \Phi = 0.8771 \Rightarrow n/n' = 393 \pm 7$). This discontinuity results from the larger density of reflected particles as compared to transmitted ones than is found in the isotropic case. Especially in the case of infinitesimal pitch-angle scattering, the particles undergo repeated reflections (by which they are accelerated) before they reach a pitch angle at which they are able to cross the shock into the downstream region.

Allowing for a larger maximum value in the change of the pitch angle increases the probability of entering the loss cone per scattering event, and therefore crossing the shock from upstream to downstream. This reduces the density contrast (Fig. 7). The effect on the spectral index is restricted to a small region in the parameter $u_s/\cos \Phi$ (the intersection velocity of magnetic field and shock) (Fig. 3). The reason for this steepening is that the acceleration due to reflections becomes less effective. For large pitch-angle scattering where the pitch angle is randomised after every scattering event, the pile-up effect is almost absent, and the minimal spectral index (the flattest spectrum) which can be reached at oblique shocks with non-relativistic shock velocities is $s \gtrsim 3.4$ (see also N&T95).

In the case of non-relativistic particles accelerated at solar system shocks, a significant density peak can occur only for highly oblique magnetic fields for particles whose velocity is less than an order of magnitude greater than the intersection velocity of shock and magnetic field. The occurrence of a density peak of accelerated particles at the shock front could in

principle be detected in situ by space observations in the solar system, so that it is important to determine whether effects such as modification of the velocity profile by the pressure of accelerated particles can affect our results. Simulations of this nonlinear problem have been performed by Ellison et al. (1996). However, they detect no difference in the spectral index between runs with infinitesimal and large pitch-angle scattering, whereas we predict that a difference should accompany a high density peak ahead of the shock front, as discussed in Sec. 3.1. Very recently, numerical solutions of the transport equation for mildly relativistic particles at solar system shocks have found a density peak at the shock front (Ruffolo 1999).

A pile-up of electrons ahead of the blast-wave associated with a supernova remnant could cause a synchrotron flux which *decreases* downstream of the shock instead of increasing due to the compression of the magnetic field (O91). Whereas this could always happen at a shock which propagates in an inhomogeneous medium, such a signature could be also produced by a shock moving in a homogeneous interstellar medium with an oblique magnetic field as a result of a pile-up of reflected particles.

The synchrotron emission as a function of frequency scales as $\epsilon(\nu) \propto n\nu^{-\alpha} B^{\alpha+1}$, where $\alpha = (s - 3)/2$. Because of the enhanced synchrotron emission due to the increasing magnetic field downstream of the shock, the observation of the density peak upstream of an oblique shock would be possible only for very high obliquities observed at high angular resolution. For a typical supernova shock velocity of $u_s = 7000 \text{ km s}^{-1}$, an upstream inclination angle of $\Phi \gtrsim 88^\circ$ leads to an upstream density (of highly relativistic particles) which exceeds by more than a factor 10 the downstream density $n/n' \gtrsim 10$ (see Fig. 6 for infinitesimal, and Fig. 7 for intermediate pitch-angle scattering). At the same time the very flat spectrum produced by these particles ($s \approx 3$) leads to only a linear enhancement of the downstream synchrotron emission due to the compressed magnetic field, $(B/B')^{\alpha+1} \approx 1/4$ (for $r = 4$). This means that the synchrotron emission upstream would exceed the emission downstream. We estimate that such an effect could be resolved in the radio range and for parameters typical of a young SNR such as Tycho if the scattering frequency ν_s , defined in Eq. (14), is smaller than the gyro-frequency by a factor of roughly 10^3 .

Observations of the Tycho supernova remnant have revealed a density peak in the vicinity of the blast wave (Reynoso et al. 1997), which cannot be understood by the theory of an unmodified parallel shock moving in a homogeneous medium. At least *one* of these assumptions must be dropped in a model of that part of the remnant which shows this feature. A highly oblique shock is a possibility, especially if nonlinear effects in the precursor cause preferential alignment of the field in the plane of the shock, as suggested by recent simulations (Bell, private comm.). However, the observed spectral indices of young shell-like supernova remnants are in the range $0.5 \lesssim \alpha \lesssim 0.8$ (Reynolds & Ellison 1992), which corresponds to $4 \lesssim s \lesssim 4.6$ and deviates from the standard result for compression $r = 4$ at a highly oblique shock. Spectral indices in this regime can be produced by stochastic perpendicular magnetic fields (Kirk et al. 1996; Gieseler 1998)

or strongly modified oblique shocks (Reynolds & Ellison 1992). Whereas in the former case a density peak ahead of the shock does not arise (Gieseler 1998), in the latter case the pile-up of accelerated particles may be an important effect. Alternatively, nonlinear hydrodynamic effects of the accelerated particles can create an unstable density spike downstream of the shock, as shown by Jun & Jones (1997), which may be responsible for the enhancement in the synchrotron emission.

We have shown that highly oblique shocks can produce a pronounced density peak due to a pile-up of accelerated particles ahead of the shock front. In Monte-Carlo simulations, this might appear as a discontinuity or even be overlooked, depending on the method used and the spatial resolution achieved. We point out that the nonlinear effects of such a pile-up could be significant, so that it is important to locate this effect in simulations which incorporate the reaction of the pressure of accelerated particles on the plasma dynamics.

Acknowledgements. This work was supported by the European Commission under the TMR programme, contract number FMRX-CT98-0168. U.D.J.G. acknowledges support from the Deutsche Forschungsgemeinschaft under SFB 328.

References

- Achterberg A., Norman C.A., 1980, *A&A* 89, 353
 Axford W.I., Leer E., Skadron G., 1977, Proc. 15th. Int. Cosmic Ray Conf., Plodiv, 11, p. 132
 Axford W.I., 1981, Proc. 17th. Int. Cosmic Ray Conf., Paris, 12, p. 155
 Baring M.G., Ellison D.C., Jones F.C., 1993, *ApJ* 409, 327
 Begelman M.C., Kirk J.G., 1990, *ApJ* 353, 66
 Bell A.R., 1978, *MNRAS* 182, 147
 Blandford R.D., Eichler D., 1987, *Physics Reports* 154, 1
 Blandford R.D., Ostriker J.P., 1978, *ApJ* 221, L29
 Decker R.B., 1988, *Space Sci. Rev.* 48, 195
 Drury L.O'C., 1983, *Rep. Prog. Phys.* 46, 973
 Ellison D.C., Baring M.G., Jones F.C., 1996, *ApJ* 473, 1029
 Gieseler U.D.J., 1998, *Transport und Beschleunigung von Teilchen in astrophysikalischen Plasmen*. Dissertation, Ruprecht-Karls-Univ. Heidelberg, MPI für Kernphysik, preprint MPI H-V6-1998
 de Hoffmann F., Teller E., 1950, *Phys. Rev.* 80, 692
 Jokipii J.R., 1971, *Review of Geophysics and Space Physics* 9, 27
 Jun B.-I., Jones T.W., 1997, *ApJ* 481, 253
 Kirk J.G., Duffy P., Gallant Y.A., 1996, *A&A* 314, 1010
 Kirk J.G., Heavens A.F., 1989, *MNRAS* 239, 995 (K&H89)
 Kirk J.G., Melrose D.B., Priest E.R., 1994, In: Benz A.O., Courvoisier T.J.-L. (eds.) *Plasma Astrophysics*. Saas-Fee Advanced Course 24, Springer-Verlag, Berlin
 Kirk J.G., Schneider P., 1987, *ApJ* 322, 256
 Krymskii G.F., 1977, *Sov. Phys. Dokl.* 22, 327
 Naito T., Takahara F., 1995, *MNRAS* 275, 1077 (N&T95)
 Ostrowski M., 1991, *MNRAS* 249, 551 (O91)
 Reynolds S.P., Ellison D.C., 1992, *ApJ* 399, L75
 Reynoso E.M., Moffett D.A., Goss W.M., et al., 1997, *ApJ* 491, 816
 Ruffolo D., 1999, to appear in *ApJ* 515, also available as astro-ph/9812064
 Skilling J., 1975, *MNRAS* 172, 557
 Spatschek K.H., 1990, *Theoretische Plasmaphysik*. Teubner Verlag, Stuttgart
 Terasawa T., 1979, *Planet. Space Sci.* 27, 193
 Webb G.M., Axford W.I., Terasawa T., 1983, *ApJ* 270, 537
 Whipple E.C., Northrop T.G., Birmingham T.J., 1986, *J. Geophys. Res.* 91, 4149